INDUCED PLURIPOTENT STEM CELL-DERIVED MESENCHYMAL STEM CELLS-DERIVED EXTRACELLULAR VESICLES ATTENUATE LPS-INDUCED LUNG INJURY AND ENDOTOXEMIA IN MICE

Qinghe Meng¹, Tackla Winston², Julia Ma³, Yuanhui Song², Chunyan Wang¹, Junhui Yang²,

Zhen Ma^{2#}, Robert N Cooney^{1#}

¹Department of Surgery, State University of New York (SUNY), Upstate Medical University, Syracuse, New York;

²Department of Biomedical & Chemical Engineering, Syracuse University, Syracuse, New York; ³Department of Medicine, State University of New York (SUNY), Upstate Medical University, Syracuse, New York

#Corresponding Authors:

Zhen Ma PhD

Department of Biomedical & Chemical Engineering

Syracuse University

318 Bowne Hall

120 Sims Dr.

Syracuse, NY 13244

Tel. (315) 443-4057

E-mail: zma112@syr.edu

Robert N. Cooney, MD

Department of Surgery

SUNY Upstate Medical University

750 E Adams St., Suite 8141

Syracuse, NY 13210

Tel. (315) 464-5549

FAX: (315) 464-6250

E-mail: cooneyr@upstate.edu

Abstract

Introduction: We hypothesized extracellular vesicles (EVs) from preconditioned human induced pluripotent stem cell-derived mesenchymal stem cells (iMSCs) attenuate LPS-induced acute lung injury (ALI) and endotoxemia.

Methods: iMSCs were incubated with cell stimulation cocktail (CSC) and EVs were isolated. iMSC-EVs were characterized by size and EV markers. Bio-distribution of intratracheal (IT), intravenous and intraperitoneal injection of iMSC-EVs in mice was examined using IVIS. Uptake of iMSC-EVs in lung tissue, alveolar macrophages and RAW264.7 cells was also assessed. C57BL/6 mice were treated with IT/IP iMSC-EVs or vehicle ± IT/IP LPS to induce ALI/ARDS and endotoxemia. Lung tissues, plasma and BALF were harvested at 24 h. Lung histology, BALF neutrophil/macrophage, cytokine levels and total protein concentration were measured to assess ALI and inflammation. Survival studies were performed using IP LPS in mice for three days.

Results: iMSC-EV route of administration resulted in differential tissue distribution. iMSC-EVs were taken up by alveolar macrophages in mouse lung and cultured RAW264.7 cells. IT LPS-treated mice demonstrated marked histologic ALI, increased BALF neutrophils/macrophages and protein, increased BALF and plasma TNF- α /IL-6 levels. These parameters were attenuated by 2 h pre- or 2 h post-treatment with IT iMSC-EVs in ALI mice. Interestingly, the IT LPS-induced increase in IL-10 was augmented by iMSC-EVs. Mice treated with IP LPS showed increases in TNF- α and IL-6 that were downregulated by iMSC-EVs and LPS-induced mortality was ameliorated by iMSC-EVs. Administration of IT iMSC-EVs 2 h after LPS down-regulated the increase in pro-inflammatory cytokines (TNF- α /IL-6) by LPS and further increased IL-10 levels. **Conclusions:** iMSC-EVs attenuate the inflammatory effects of LPS on cytokine levels in ALI and IP LPS in mice. LPS-induced mortality was improved with administration of iMSC-EVs.

Key Words: ALI, ARDS, Endotoxemia, Extracellular vesicles (EVs), Induced mesenchymal stem cells (iMSCs), Inflammation.



Introduction

Acute respiratory distress syndrome (ARDS) is a life-threatening condition caused by direct or indirect lung injury characterized by severe inflammation, capillary leak, alveolar flooding and hypoxemia. Despite advances in critical care and protective mechanical ventilation, ARDS continues to pose a significant clinical challenge, with high mortality rates and limited treatment options. The quest for novel and effective therapeutic strategies to mitigate the devastating impact of ARDS remains a priority in the field of critical care medicine. Previous studies using anti-inflammatory agents, surfactant, nitric oxide in ARDS demonstrate conflicting results (1). More recently, mesenchymal stromal cells have shown promising results in experimental and human ARDS, but the recently reported START trial showed no benefit in Covid-19 related ARDS (2).

Stem cell therapies are widely used in regenerative medicine and are considered an attractive option for treating various lung diseases and sepsis (3-5). Despite these positives, the disadvantages of stem cell based therapies including immune reactions, tumorigenicity, and infection transmission (6). The paracrine effects of stem cells represent the most important mechanism for their immunomodulatory and regenerative properties (7-10). Extracellular vesicles (EVs), especially exosomes (30-150 nm in diameter), are secreted by stem cells and contain multiple bioactive molecules (proteins, lipids, nucleic acids, and membrane receptors of the cells from which they originate) are recognized as important mediators of their paracrine effects through the transfer of biological cargos (10-12). EVs provide multiple advantages for clinical applications in pulmonary disease because they have: 1. Small size suitable for delivery and deposition in small airways and alveolar areas by inhalation therapy. 2. Lipid bilayer

structure which attenuates their degradation in tissues and body fluids, and 3. lower levels of immunogenicity and toxicity compared to cell therapies. Furthermore, EVs can be modified and loaded with drugs of interest, and their surface-specific receptors can be artificially engineered to target specific cells or tissues (13-15).

Various types of stem cell-derived EVs, such as mesenchymal stem cells (MSCs), have been studied in experimental models and clinical trials for respiratory diseases including ALI and ARDS (16-18). MSC-EV treatment is correlated with lower mortality in experimental animal models of sepsis (19). Additionally, EV-based therapies, especially mesenchymal stem cell-derived EVs, are being intensively studied for the treatment of COVID-19 (20,21). According to the results of completed and ongoing ALI/ARDS clinical trials, EVs are a promising therapy for ALI/ARDS patients although more randomized controlled studies are needed to prove their safety and efficacy (9).

While EVs derived from primary MSC hold significant promise for treating ALI/ARDS, several challenges must be addressed to maximize their therapeutic potential, such as therapeutic efficacy and safety, scale-up/manufacturing, heterogeneity, storage and stability and cargo variability. Studies have shown that while the majority of MSCs derived from tissues align with International Society for Cell Therapy (ISCT) criteria, they exhibit significant heterogeneity in terms of proliferation, differentiation capacity, and immunomodulatory potential. This variability is a detriment to their clinical application and potentially accounts for the conflicting outcomes observed in clinical trials (22). Consequently, finding alternative sources of MSCs that address the limitations associated with tissue-derived MSCs is a research priority in this field.

MSCs derived from human induced pluripotent stem cells (iMSCs) based on different protocols (23-25) are expected to overcome these limitations and serve as a reproducible and sustainable source of cells (26-29). The production of scalable EVs from iMSC (iMSC-EVs) with reduced heterogeneity and variability, as well as enhanced immunomodulatory and regenerative capabilities, enable the creation of a novel therapeutic solution to ALI/ARDS and sepsis. We have successfully developed a robust serum-free protocol allowing for consistent iMSC differentiation through an intermediate neural crest stage (30,31). Simplified procedures for differentiation and modular fabrication, coupled with serum-free culture conditions, enable large-scale production of MSCs and MSC-EVs. Since MSC-specific biomarkers detected from iMSC and primary MSC have been shown to be consistent, it is of great interest to study their biological functions, particularly EVs derived from iMSCs. Thus, the aim of this study is to determine whether prophylactic and therapeutic administration of iMSC-EVs can attenuate inflammation, prevent lung injury and impact survival in experimental murine models of LPSinduced ARDS and endotoxemia. Our results provide evidence that administration of IT iMSC-EVs are taken up and attenuate lung inflammation in murine ARDS. We also show that IP administration of iMSC-EVs attenuates inflammation and reduces mortality in murine IP LPSinduced endotoxemia.

Materials and Methods

Animal care, endotoxemia and lung injury model

Male and female mice 7-9 weeks of age were used in the experiments below and were bred from C57BL/6 mice obtained from Jackson Laboratories (Bar Harbor, ME). All mice were housed under controlled conditions, including a temperature of 22°C and a photoperiod of 12

hours of light and 12 hours of darkness. They had unrestricted access to a standard diet (Lab Diet 5008, St. Louis, MO) and free access to water. All the experimental animal procedures in this study were reviewed and approved by the Institutional Animal Care and Use Committee of SUNY Upstate Medical University (IACUC # 344). The experiments adhered strictly to the guidelines outlined by the National Institutes of Health and the ARRIVE guidelines pertaining to the ethical use of laboratory animals.

Mouse model of endotoxemia: Intraperitoneal injection of LPS was used to induce endotoxemia in mice. This mouse model has been used to recapitulate human sepsis for nearly 100 years since it was first described to replicate most pathophysiologic features of severe sepsis following induction with LPS (32). A lower dose of LPS (5 mg/kg) was used to induce a less severe form of sepsis to study inflammatory responses, cytokine production, and cellular changes associated with sepsis. After the mice received LPS, they were observed for 24 hours and then euthanized to collect samples for further analysis. A higher dose of LPS (15 mg/kg) was used to replicate severe endotoxemia and determine the effects of iMSC-EVs on mortality. Mice were monitored for 3 days for survival.

Mouse model of ALI/ARDS: Mice in both the LPS and control groups were anesthetized using IP injection of ketamine (80 mg/kg) and xylazine (8 mg/kg). Once anesthetized the mice were positioned in the supine posture on an intubation platform. A fiber optic illuminator was positioned over the trachea, the tongue was gently retracted upward and to the left to facilitate visualization of the larynx. The administration of LPS (2.5 mg/kg) and saline solutions (ensuring that the volume for each mouse did not exceed 70 µl) was performed using a MicroSprayer

aerosolizer needle (Catalog Number: YAN30012, Shanghai Yuyan Instrument Co., Ltd.) following insertion into the tracheal lumen. Following IT administration of LPS or saline, mice were observed for 24 hours, then euthanized to collect BALF, blood and lung tissue for subsequent analysis. IT LPS injection is a well-established experimental model of ALI/ARDS in mice to study the pathophysiology of ARDS, characterized by neutrophil infiltration and endothelial cell damage (33). Of note, the dosage of intratracheal LPS administered in this study did not result in any mortality among the experimental groups.

Derivation of mesenchymal stem cells from hiPSCs (iMSCs)

Differentiation and maintenance of the human induced pluripotent stem cell (hiPSCs) into iMSCs have been previously described (30). Briefly, the hiPSCs were seeded on Geltrex-coated 6-well plates and maintained in Essential 8 (E8) media (Life Technologies, Cat. #: A1517001). Next, hiPSCs were differentiated into neural crest cells using a specified differentiation media consisting of 10 ng/mL bFGF (R&D Systems, Cat. #: 233-FB), 4 μM SB431542 (Stemgent, Cat #: 04-0010-10), and 4 μM WNT agonist CHIR99021 (CHIR) (Stemgent, 04-2004) in Essential 6 (E6) media (Life Technologies, Cat. #: A1516401). The neural crest cells were differentiation into iMSCs using StemPro MSC SFM media (Life Technologies, Cat. #: A1033201) for 18 days.

Isolation of iMSC-EVs

Differentiated iMSC cells are cultured in a complete growth medium (DMEM supplemented with 10% FBS and 1% penicillin-streptomycin) at 37°C with 5% CO₂. Once iMSCs reached 70-80% confluence, culture medium was replaced with serum-free DMEM, and cells were incubated with cell stimulation cocktail (CSC), containing phorbol 12-myristate 13-acetate

(PMA), ionomycin, brefeldin A and monensin (Life Technologies, Cat. #: 00-4970-03) for 3 days to promote EV secretion. Conditioned media were then collected and centrifuged at 300 × g for 10 minutes to remove cell debris, and then concentrated using Amicon 100 kDa ultracentrifugation filters at 4000 × g for 20 minutes. The samples are collected and incubated with 0.5 volumes of Total Exosome Isolation Reagent (Life Technologies, Cat. #: 4478359) per manufacturer's instruction. The suspension was vortexed thoroughly to form a homogenous solution, and then incubated overnight in the refrigerator. The next day, samples were centrifuged at 2°C, 10,000 × g for an hour and the supernatant was discarded. The pellet was resuspended in sterile DPBS, and further filtered by size exclusion chromatography using qEV columns (qEVoriginal/35 nm Gen 2 Column, IZON Inc.) with an optimum recovery range of 35 nm to 350 nm.

Characterization of iMSC-EVs

1) EV samples for Cryogenic electron microscopy (cryo-EM). An aliquot of 3 μL of the aqueous sample was applied on glow-discharged (30 s, 30 mA) lacey carbon EM grids, blotted for 2 seconds, and then plunge-frozen into liquid ethane using Vitrobot Mark IV (FEI, USA). The samples were imaged in a transmission electron microscope (TEM) (Thermo Fisher Talos Arctica) equipped with K3 direct electron detector camera and Bioquantum Imaging filter (GATAM Metek), which is optimized for high-throughput, high-resolution imaging of single-particle cyro-EM. The equipment is equipped with an autoloader allowing up to 12 grids to be loaded under liquid nitrogen and vacuum condition and a stable stage for imaging at cyrogenic condition with high tilt for tomography. Automated data collection for single-particle cyro-EM is completed by Smart EPU software (ThermoFisher Scientific). 2) Size Distribution: The size

distribution of iMSC-EVs was determined by dynamic light scattering (DLS) using a Zetasizer Nano ZS90 (Malvern Instruments). The MSC-EV suspension was diluted in PBS, and measurements were performed at 25°C. *3) EV Marker Expression:* Western blot analysis was conducted to assess the presence of EV markers CD9, CD63, CD81 and HSP90α/β in iMSC-EVs.

iMSC-EV bio-distribution by different routes of administration

To enable non-invasive real-time tracking of iMSC-EVs in living animals, IVIS 50 (PerkinElmer) with the excitation/emission at 784/806 nm was used to longitudinally monitor iMSC-EV trafficking in living animals and organs after the iMSC-EVs were labeled using the kit from System Biosciences (Cat. #: EXOGV900A-1) following manufacturer's guidelines. Briefly, 2 μl of ExoGlowTM-Vivo dye (Near IR) was added into 200 ug protein equivalent of EVs (by BCA assay) in 500 μl 1X PBS, then incubated for 1 h at RT. Purification of the EVs from the labeling reaction using ExoQuick-TC reagent. Labeling efficiency analysis was performed using Thin-layer chromatography (TLC). Signals were detected 24 hours after dosing by different routes of administration (IT, IV and IP).

iMSC-EV treatment and tissue harvest

iMSC-EVs (at a dose of 0.6 mg/kg) or vehicle were administered prophylactically 2 hours prior to the induction of ALI/ARDS or endotoxemia as described above. 24 hours later the mice were euthanized under anesthesia. Samples of blood (EDTA as an anticoagulant), lung tissue (either fixed in 10% formalin for histological analysis or frozen for protein analysis), and bronchoalveolar lavage fluid (BALF) were collected for subsequent analysis. To investigate the therapeutic impact of iMSC-EVs on ALI/ARDS, we also administered iMSC-EVs 2 hours

following IT administration of LPS. After 24 hours of LPS, samples were collected as described above.

Cytological and protein analysis in BALF

Bronchoalveolar lavage fluid (BALF) was collected from the mouse lung by lavage using 3 sets of 0.5 ml sterile saline washes. Collected fluid was centrifuged at 250×g for 10 minutes. The resulting pellet was then resuspended in 1 ml of sterile saline. To prepare cell slides for analysis, 100 μL of the cell suspension was subjected to centrifugation using a Cytospin centrifuge (Hettich ROTOFIX 32A) at 1000 rpm for 3 minutes, effectively mounting the cells onto a slide. After mounting, the slide was left to air-dry and was subsequently stained with Hema-3 (Fisher Scientific, Kalamazoo, MI) for further examination. Neutrophils and macrophages present in the cell preparations were quantified by blinded reviewers, who assessed 20 high-power fields (HPF) using a Nikon Eclipse TE2000-U microscope (Nikon, Melville, NY). Bicinchoninic acid (BCA) assay was used to check protein concentration in BALF.

Uptake of iMSC-EVs in lung tissue and Raw264.7 macrophages

iMSC-EVs were labeled using ExoGlowTM-Vivo dye as described above. 50 μl of labeled iMSC-EVs were delivered into mice by IT. Lung tissue was collected after 24 h. Fresh lung tissue was embedded and frozen in OCT. Sections were cut at 5 μm thick in the cryostat at -20°C. BALF was obtained from mouse lung and cell slides were prepared using the procedure mentioned above.

Raw264.7 cells were incubated in growth medium with labeled EVs for 4 h in 96-well plate. Then cells were washed with PBS twice for detection of EV uptake. TE2000-U research microscope (Nikon, Melville, NY) was used s used to image uptake of iMSC-EVs.

Western blot and ELISA

Frozen lung tissue was homogenized using RIPA buffer and the extracted protein was utilized for Western blot analysis. A BCA micro assay kit (Cat. #: 23235, Thermo Scientific, Rockford, IL) was used to measure the total protein concentrations in lung tissue and bronchoalveolar lavage fluid (BALF). For the Western blot procedure, 20 μg of protein was separated via SDS-PAGE gel and subsequently transferred onto PVDF membranes from Millipore Co., Ltd. The membranes were initially incubated with a solution of 5% non-fat milk (Bio-Rad Laboratories) in Tris-buffered saline with 0.5% Tween-20 (TBS-T) for one hour at RT. Following this, incubation continued overnight at 4°C with primary antibodies sourced from Santa Cruz Biotechnology, which included CD-63 (Cat. #: 5275, 1:500), CD-81 (Cat. #: sc-7637, 1:500), CD 9 (Cat. #: sc-166029, 1:500) and HSP90α/β (Cat. #: 13119, 1:500). Secondary antibody linked to horseradish peroxidase (HRP), acquired from Bio-Rad Laboratories (Cat. #: 1662408), was applied for one hour at RT. The antibody-antigen complexes were visualized using the ECL method following the manufacturer's instructions.

Collected plasma and BALF samples were employed to assess the levels of TNF-α (Cat. #: 88-7324-22, Invitrogen), IL-6 (Cat. #: 88-7064-88, Invitrogen) and IL-10 (Cat. #: BMS614INST, Invitrogen). The quantification of these cytokines was carried out using commercial ELISA kits, following the manufacturer's instructions.

Histological assessment of lung injury

The lung tissues were fixed for histological examination by gently introducing 0.5 ml of 10% neutral formalin through the trachea for inflation-fixation. Subsequently, fixed lung specimens were embedded in paraffin. Sections 5 µm in thickness were prepared from the lung tissue samples and subjected to hematoxylin and eosin (H&E) staining. Histopathological assessment of acute lung injury was performed using the 0–2 scoring system as previously described (34). Briefly, neutrophils in the alveolar and interstitial spaces were counted separately. Hyaline membranes, void-filling protein fragments, and septal thickening were evaluated. To derive the lung injury score, the sum of these five distinct parameters was calculated, with each feature being weighted based on its relevance. The resulting score was then normalized to the number of fields that were evaluated. A total of 20 high-power field (HPF) counts were performed on three representative fields from each slide using a light microscope at 400× magnification, with two pathologists conducting these assessments in a blinded manner.

Statistical analysis

Data are expressed as mean ± SE. Statistical analysis of data was performed using GraphPad Prism software (version 5.0). Sample sizes for each experimental group (n = 5-10) are indicated in the figure legends. Differences between groups were determined using one-way analysis of variance (one-way ANOVA) with Bonferroni multiple comparisons test. The difference between groups was considered significant when P<0.05. All data are from three or more independent experiments.

Results

Characterization of iMSC-EVs

- 1. Cyro-EM was used to visualize the morphology of iMSC-EVs. Images revealed the presence of small, spherical vesicles with a typical lipid bilayer structure, consistent with the expected morphology of EVs (**Supp. Fig. 1A**, http://links.lww.com/SHK/B938).
- 2. DLS analysis was performed to determine the size distribution of iMSC-EVs. The majority of iMSC-EVs had a diameter ranging from 30 to 150 nanometers (**Supp. Fig. 1B**, http://links.lww.com/SHK/B938). This size range is characteristic of exosomes, a subtype of EVs.
- 3: EV marker expression: To confirm the identity of MSC-EVs, we assessed the expression of specific EV markers using Western blot analysis. Our results demonstrated the presence of classical EV markers, including CD9, CD63, CD81 and HSP90α/β in MSC-EVs (**Supp. Fig. 1C**, http://links.lww.com/SHK/B938).

Biodistribution and uptake of iMSC-EVs

To determine how the route of administration (IP, IV and IT) impacts the uptake of iMSC-EVs by different tissues over time we labeled them with Near-IR dye and injected them in mice as described. *In vivo* fluorescence imaging was performed at different time points and revealed a dynamic pattern of iMSC-EV distribution that varied by route of administration (**Supp. Fig. 2**, http://links.lww.com/SHK/B939). Mice were sacrificed at 24 h and tissues (lungs, heart, liver,

spleen, kidney and intestines) were harvested for analysis. As shown in **Figure 1**, the route of administration had a significant impact on signal intensity in different organs. The IT route of administration resulted in strong signals throughout the lungs and liver, a modest signal in the kidneys with a small signal in the stomach (**Fig. 1A**). IP administration resulted in strong signals in the liver and kidneys, a modest signal in spleen and faint gastric signal (**Fig. 1B**). IV administration resulted in strong uptake in liver and kidney with modest uptake in stomach (**Fig. 1C**). Based on this data we used the IT route of administration for iMSC-EVs in our experiments on ALI/ARDS and the IP route of administration for the intraperitoneal LPS "sepsis" experiments.

Uptake of iMSC-EVs in mouse lung tissue and macrophages

To further characterize the uptake of iMSC-EVs in lung tissue we examined sections of lung tissue histologically following IT administration of fluorescence-labeled iMSC-EVs in mice. As shown in **Fig 2A**, our examination of lung sections revealed the presence of iMSC-EV-derived fluorescence signals in lung parenchyma indicating that iMSC-EVs are taken up by the pulmonary parenchyma following IT administration. Next, we examined the uptake of iMSC-EVs in alveolar macrophages isolated from mice following IT injection of labeled iMSC-EVs (**Fig. 2B**) and in cell culture experiments with Raw264.7 macrophages incubated with labeled iMSC-EVs (**Fig. 2C**). Alveolar macrophages isolated from mice (**Fig. 2B**) demonstrate significant uptake (**Fig 2B**) of labeled iMSC-EVs. Cultured Raw264.7 macrophages also demonstrate substantial uptake (**Fig. 2C**) of labeled iMSC-EVs. Collectively these data provide evidence that iMSC-EVs are efficiently internalized by both alveolar and cultured macrophages.

Cytokine levels in plasma and bronchoalveolar lavage fluid (BALF)

To assess the anti-inflammatory properties of iMSC-EVs via prophylactic administration, we measured the levels of proinflammatory cytokines (TNF-α & IL-6) in plasma and BALF from the mice with IP LPS endotoxemia and IT ALI/ARDS (Fig. 3). Plasma levels of TNF-α and IL-6 were markedly increased (Fig 3A, B) in the IP LPS mice (P<0.05, Vehicle vs. LPS). Prophylactic treatment with iMSC-EVs significantly attenuated the increase in both plasma TNF-α (Fig. 3A) and IL-6 (Fig. 3B) in IP LPS treated mice (P<0.05, LPS vs. LPS/iMSC-EVs). Consistent with this finding, mice treated with IT LPS to induce ALI/ARDS demonstrate a marked increase in both TNF-α and IL-6 in plasma (Fig. 3C & 3D) and BALF (Fig. 3E and 3F). Pretreatment with IT iMSC-EVs significantly attenuated the increases in TNF-α and IL-6 observed in the IT LPS ALI/ARDS model (P<0.05, LPS vs LPS/iMSC-EVs). In contrast, IL-10, which was increased by LPS, was significantly elevated by iMSC-EVs in plasma (Fig. 3G) and BALF (Fig. 3H) in the mice with ALI/ARDS (P<0.05, LPS vs LPS/iMSC-EVs), suggesting that iMSC-EVs can also upregulate anti-inflammatory cytokines to suppress inflammation. Collectively these data provide evidence that iMSC-EVs can attenuate inflammation in LPS models of endotoxemia and ALI/ARDS.

BALF cytology and total protein concentration

Analysis of BALF is frequently used to assess the severity of lung injury in ALI/ARDS. The presence of neutrophils and macrophages reflects pulmonary inflammation and the relative abundance of BALF protein indicates the severity of the capillary leak. A 2-hour prophylactic administration of iMSC-EVs were used in this experiment. In healthy controls and mice given EVs alone (**Fig. 4**), BALF contained few WBC and relatively low levels of protein. In contrast,

IT administration of LPS resulted in a dramatic increase in neutrophils, macrophages and BALF protein (**Fig. 4**). Treatment with iMSC-EVs 2 h before IT LPS significantly attenuated the LPS-induced increase in BALF neutrophils, macrophages, and total protein concentration (P<0.05, LPS vs LPS/iMSC-EVs, P<0.05). These findings provide evidence prophylactic treatment with iMSC-EVs can reduce inflammatory cell infiltration and capillary leak induced pulmonary edema in LPS-induced ALI/ARDS.

Histologic assessment of lung injury

Lung histology was evaluated to assess the ability of iMSC-EVs with 2-hour prophylactic administration to attenuate LPS-induced ALI. Representative lung histology from each group is shown in **Fig. 5A**. Lung tissue from the Control and iMSC-EV groups was essentially normal. Histologic analysis of lung tissue from LPS-treated mice demonstrates significant neutrophil infiltration, alveolar hemorrhage/edema, proteinaceous debris filling the airspaces and alveolar septal thickening compare with the Control group. Pretreatment with IT iMSC-EVs significantly attenuated both LPS-induced histologic lung injury (Fig. 5A) and lung injury score (**Fig. 5B**).

Analysis of endotoxemia-induced mortality by LPS

To assess the impact of iMSC-EVs by 2-hour prophylactic administration on survival in endotoxemia we used an "high mortality" murine IP LPS model of endotoxemia. Kaplan-Meier curves (**Fig. 6**) were generated to plot survival over time in the Control, LPS and LPS/iMSC-EV groups. The control group had 100% survival over 72 h. The LPS group demonstrated a steep decline in survival over time with a mortality rate of 80% at 72 h. In contrast, the LPS/iMSC-EVs group showed a significant improvement in survival with a mortality rate of 60% at 72 h.

These findings provide evidence that pretreatment with iMSC-EVs can improve survival in high acuity LPS murine endotoxemia models.

Therapeutic effects of iMSC-EVs in ALI/ARDS by LPS

The effects of iMSC-EV administration on ALI following the LPS-induced injury model were investigated to test the therapeutic effects of iMSC-EVs on ALI (**Fig** 7). The LPS-induced increase in pro-inflammatory cytokines (TNF-α/IL-6) in BALF (**Fig.** 7A₁ & 7A₂) and plasma (**Fig.** 7A₃ & 7A₄) were ameliorated by iMSC-EVs. In contrast, the increase in IL-10 in BALF (**Fig.** 7A₅) and plasma (**Fig.** 7A₆) caused by LPS was augmented by iMSC-EVs. Post-treatment with iMSC-EVs also attenuated the histologic lung injury induced by LPS (**Fig** 7B). These data provide evidence that post-injury administration of iMSC-EVs attenuate LPS-induced ALI.

Discussion

MSCs can be isolated from multiple sources including adipose tissue, bone marrow, umbilical cord, cord blood, amniotic fluid and membrane, and placental tissue (35,36). More recently, as in the current study, MSCs can be derived from pluripotent human stem cells. The tissue of origin and isolation techniques can impact many properties of MSC-EVs including size distribution, surface markers, biological contents and *in vivo* biodistribution. The current study uses iMSCs conditioned by incubation with cell stimulation cocktail containing phorbol 12-myristate 13-acetate (PMA). The conditioned iMSC-EVs were isolated using total exosome isolation reagent from Life Technologies and characterized using standard techniques including transmission electron microscopy and dynamic light scattering to confirm their size profiles. Western blots were performed to document their surface markers and cargo proteins (CD9,

CD63, CD81, HSP90). Our biodistribution studies provide evidence the IT route of administration is especially effective for enhanced uptake in lung tissue. Perhaps most importantly we demonstrate that prophylactic IT administration of iMSC-EVs significantly attenuates lung injury and inflammation, and that IP administration attenuates systemic inflammation and mortality in IP LPS-induced endotoxemia.

Our findings are consistent with multiple other studies demonstrating a therapeutic benefit of MSC-EVs in sepsis-induced organ dysfunction, including acute lung injury (10), acute kidney injury, cardiovascular disorders, and liver injury (37). The anti-inflammatory effect of EVs is one of its important properties. Our studies have demonstrated that human induced pluripotent stem cell (iPSC)-derived MSCs possess significant advantages over MSCs obtained from tissue sources. As a result, they may be considered a viable alternative cell source for stem cell-based therapies (38). More importantly, it provides a solution to avoid some of the limitations of EVs derived from primary MSCs. Based on previous studies on the role of MSC-EVs in anti-inflammation, tissue regeneration and repair, we hypothesized that EVs derived from iMSCs also have potential in immunomodulation and the intervention of lung injury. In current study, our findings provide evidence iMSC-EVs act to improve inflammation control by reducing proinflammatory cytokines, prevent lung injury by inhibiting inflammatory cell infiltration and reduce mortality by modulating systemic inflammation.

Our studies involved preconditioning cultured iMSCs with cell stimulation cocktail (CSC), a commercially available mixture of phorbol 12-myristate 13-acetate (PMA), ionomycin, brefeldin A and monensin (38). Preconditioning of MSCs with hypoxia, inflammatory stimuli and 3D

culture are common techniques to enhance the immunomodulatory, anti-inflammatory and regenerative capacity of the MSC secretome (39). Pilot studies (not shown) demonstrate that iMSC-EVs isolated from the iMSCs pretreated with either LPS or CSC significantly attenuate the inflammatory response of LPS-treated RAW264.7 cells. Based on these results, we used iMSC-EVs from CSC pretreated iMSCs in the current study. Our findings are consistent with Ti D et al. who showed that LPS preconditioning of MSCs facilitates transition of macrophages to the less inflammatory M2 phenotype (40).

Several studies have examined the impact of administration route (IV, IT, IP) on the biodistribution of MSC-EVs in different organs over time. Umbilical cord MSC-EVs were examined for their tissue localization over time after IV, IT or intranasal administration (41). Consistent with our findings, IV administration of MSC-EVs resulted in EV accumulation in liver, spleen and to a lesser extent in lung, whereas IT administration of MSC-EVs resulted in preferential localization in lung with smaller amounts in liver, and MSC-EVs via intranasal administration primarily localized in brain. Presumably the subtle differences in our tissue localization results (less EVs in lung and spleen with more in kidney after IV administration and more EVs in kidney after IT administration) are due to differences in MSC sources and other experimental differences. In another study using MSCs from bone marrow and umbilical cord, IV administration of MSC-EVs localized in liver, kidney, spleen, and lung in mice with LPSinduced ALI (42). Of interest, administering EVs after inducing lung injury (10 to 48 h later) resulted in increased accumulation of EVs in lung tissue. The findings that lung injury enhances lung uptake of MSC-EVs suggest that additional studies are needed to determine the optimal timing of MSC-EVs administration in experimental lung injury. Wiklander et al (43) compared tissue biodistribution after IV and IP administration of bone marrow-derived MSC-EVs. They noticed EV accumulation primarily in liver and spleen after IV administration, while accumulation in lung and kidney at higher EV doses. They compared IP and subcutaneous (SC) EV administration with the IV route, noting lower EV accumulation in liver and spleen after IP and SC EV administration. Our findings of iMSC-EV accumulation in liver and spleen after IP administration are consistent with Wiklander et al., except that we noted more significant EV accumulation in kidney in our study. We believe that tissue origin of EVs and route of administration significantly impact the biodistribution of EVs *in vivo*.

Lung sections from mice injected with fluorescence-labeled iMSC-EVs provide evidence for localization of EVs in cells lining the pulmonary alveoli. They also demonstrate the uptake of iMSC-EVs by primary murine alveolar macrophage and cultured macrophages (RAW264.7 cells). Alveolar macrophages play an important role in lung homeostasis and tissue repair. Our findings are consistent with previous studies suggesting the immunomodulatory effects of MSC-EVs are mediated via their paracrine effects on alveolar macrophages (44,45). Macrophages are important mediators of the host response to sepsis and our finding that RAW264.7 cells internalize iMSC-EVs is consistent with previous literature showing MSC-EVs can modulate macrophage phenotype and inflammation.

MSC-EVs contain multiple biologically active molecules that can participate in modulating the inflammatory response of the host. These include proteins, lipids, messenger RNA (mRNA), microRNA (miRNA), long noncoding RNA (lncRNA) and mitochondria. The preemptive and remedial application of iMSC-EVs mitigated the rise in pro-inflammatory cytokines (TNF-α, IL-

6) in plasma/BALF, protein levels in BALF, and histological lung tissue damage, while also amplifying the upsurge of the anti-inflammatory cytokine (IL-10) in plasma/BALF induced by LPS.

We also demonstrate that the increase in inflammatory mediators and death caused by LPS-induced endotoxemia are improved by iMSC-EVs. These findings are consistent with other studies showing significant reduction in neutrophils and macrophage inflammatory protein-2 (MIP-2) as well as modulation of macrophage polarization by MSC-EVs in murine ALI (46-50). In *in vitro* studies, MSC-EVs inhibited the secretion of pro-inflammatory factors (TNF-α, IL-1β, IL-6, IL-27), increased the concentration of the anti-inflammatory factor (TGF-β, IL-10), suppressed the differentiation of T cells into Th17 cells, and increased the level of regulatory T cells, and reduced matrix metalloproteinase-9 (MMP-9) to modulate inflammation in mouse ALI and sepsis (46,48,49,51-53). Collectively these studies support our findings that iMSC-EVs can attenuate LPS-induced direct lung injury and endotoxemia-induced indirect lung injury.

Understanding the underlying mechanisms by which MSC-EVs induce anti-inflammatory effects and improve lung injury is critical in determining their therapeutic potential. Specific miRNAs carried by MSC-EVs can target mRNAs associated with pro-inflammatory pathways, apoptosis and pyroptosis. Growing evidence suggests that numerous miRNAs are involved in fighting inflammation and repairing lung damage, including miR-377-3p (50), miR-92a-3p (54), miR-132-3p (55), miR-384-5p (56), and microRNA-130b-3p (57). Studies focused on molecules and signaling pathways have demonstrated the effects of MSC-EVs on levels of MMP-9 (51) and keratinocyte growth factor (KGF) (16), and elucidated its involvement in the regulation of

signaling pathways associated with inflammation and proliferation (e.g. NF-kB, MAPK, PI3K-AKT, STAT3 and Hippo-YAP etc.) (9). Downregulation of pyroptosis (58) and apoptosis (9) by MSC-EVs has also been reported. While pathway analysis may provide a holistic view of the molecular mechanisms underlying these immune responses, our cytokine analysis provides specific information about the presence and amount of inflammatory molecules. In the future, we hope to determine EV miRNAs expression by RNA sequencing and functional enrichment analyses.

In spite of the valuable insights gained from this study, it is essential to acknowledge its limitations, which may influence the interpretation and generalizability of the findings. These limitations include: 1) Findings from animal studies may not directly apply to humans due to differences in physiology, genetics, and metabolism although the MSCs used here were derived from human cells, 2) A detailed characterization of iMSCs and comparison to primary MSCs based on transcriptomics profile, anti-inflammatory functions, and EV properties are not included in this paper because the focus of this study is to test EV action in ALI and sepsis. A manuscript on a comparative study of EVs from both cell types is under review, 3) We only observed potential mediators 24 h after LPS administration and were unable to provide information on changes in these mediators over time. However, animal injury models induced by LPS exposure for 24 h are commonly used in other studies, 4) Our study initially used prophylactic dosing to determine the efficacy of iMSC-EVs in the treatment of ALI and endotoxemia. However, additional studies provide evidence that 2h post-LPS dosing of iMSC-EVs also attenuated ALI. Post-dosing more accurately reflects the clinical situation and translational relevance. In contrast, prophylactic dosing provides controlled experimental

conditions to ensure consistency and reproducibility of results, reduce confounding factors arising from the disease process, and facilitates accurate assessment of treatment. However, EV uptake by the lungs may be altered by lung injury, therefore additional studies on EV uptake and biodistribution of EV administration are needed.

MSC-EVs can modulate immune responses by suppressing inflammation, promoting immune tolerance, and modulating the activity of various immune cells. Secondly, MSC-EVs play a crucial role in tissue repair and regeneration by promoting cell proliferation, migration, and differentiation as well as extracellular matrix remodeling. They stimulate the regeneration of damaged tissue and accelerate the wound healing process (59). Finally, MSC-derived EVs can protect cells from apoptosis (programmed cell death) by providing anti-apoptotic factors and promoting cell survival pathways (9). iMSC-EVs exhibit diverse biological activities in addition to their anti-inflammatory effects. Our unpublished data has been shown to improve cell viability and regulate apoptosis in blood cells from sepsis patients (The data will be reported at 47th Annual Conference on Shock).

In conclusion, prophylactic IT administration of iMSC-EVs was associated with improvement in experimental LPS-induced ARDS and endotoxemia. This study confirms that EVs derived from iMSCs have anti-inflammatory function and repair lung injury via IT/IP administration in ALI and endotoxemia models, providing evidence to overcome the limitations of large-scale production of EVs and optimize conditions for treating ALI/ARDS with EVs. These findings will contribute to unlocking the vast therapeutic potential of MSC-EVs in addressing human diseases.

Acknowledgments

This work is supported by the NSF [MCB-2229111] and NIH [R01HD101130]. The authors thank Dr. Mariena Silvestry Ramos for Cyro-EM imaging at Cornell Center for Materials Research at Cornell University. They also thank Dr. Juntao Luo PhD and Dr. Dandan Guo PhD for kindly providing support in checking size distribution and labeling efficiency iMSC-EVs.

References

- 1. Jain R, DalNogare A. Pharmacological therapy for acute respiratory distress syndrome. *Mayo Clin Proc.* 2006;81(2):205-212.
- 2. Bowdish ME, Barkauskas CE, Overbey JR, et al. A Randomized Trial of Mesenchymal Stromal Cells for Moderate to Severe Acute Respiratory Distress Syndrome from COVID-19. *Am J Respir Crit Care Med.* 2023;207(3):261-270.
- 3. Wang YY, Li XZ, Wang LB. Therapeutic implications of mesenchymal stem cells in acute lung injury/acute respiratory distress syndrome. *Stem Cell Res Ther*. 2013;4(3):45.
- 4. Glassberg MK, Minkiewicz J, Toonkel RL, et al. Allogeneic Human Mesenchymal Stem Cells in Patients With Idiopathic Pulmonary Fibrosis via Intravenous Delivery (AETHER): A Phase I Safety Clinical Trial. *Chest.* 2017;151(5):971-981.
- 5. Laroye C, Gibot S, Huselstein C, Bensoussan D. Mesenchymal stromal cells for sepsis and septic shock: Lessons for treatment of COVID-19. *Stem Cells Transl Med*. 2020;9(12):1488-1494.
- 6. Lukomska B, Stanaszek L, Zuba-Surma E, Legosz P, Sarzynska S, Drela K. Challenges and Controversies in Human Mesenchymal Stem Cell Therapy. *Stem Cells Int.* 2019;2019:9628536.
- 7. Zhou Y, Yamamoto Y, Xiao Z, Ochiya T. The Immunomodulatory Functions of Mesenchymal Stromal/Stem Cells Mediated via Paracrine Activity. *J Clin Med*. 2019;8(7).
- 8. Menasche P. Cell therapy trials for heart regeneration lessons learned and future directions. *Nat Rev Cardiol.* 2018;15(11):659-671.

- 9. Liu C, Xiao K, Xie L. Advances in the use of exosomes for the treatment of ALI/ARDS. *Front Immunol.* 2022;13:971189.
- 10. Xu B, Chen SS, Liu MZ, Gan CX, Li JQ, Guo GH. Stem cell derived exosomes-based therapy for acute lung injury and acute respiratory distress syndrome: A novel therapeutic strategy. *Life Sci.* 2020;254:117766.
- 11. Mathieu M, Martin-Jaular L, Lavieu G, Thery C. Specificities of secretion and uptake of exosomes and other extracellular vesicles for cell-to-cell communication. *Nat Cell Biol*. 2019;21(1):9-17.
- 12. Thery C, Witwer KW, Aikawa E, et al. Minimal information for studies of extracellular vesicles 2018 (MISEV2018): a position statement of the International Society for Extracellular Vesicles and update of the MISEV2014 guidelines. *J Extracell Vesicles*. 2018;7(1):1535750.
- 13. Yin K, Wang S, Zhao RC. Exosomes from mesenchymal stem/stromal cells: a new therapeutic paradigm. *Biomark Res.* 2019;7:8.
- 14. Abreu SC, Weiss DJ, Rocco PR. Extracellular vesicles derived from mesenchymal stromal cells: a therapeutic option in respiratory diseases? *Stem Cell Res Ther*. 2016;7(1):53.
- 15. Riazifar M, Pone EJ, Lotvall J, Zhao W. Stem Cell Extracellular Vesicles: Extended Messages of Regeneration. *Annu Rev Pharmacol Toxicol*. 2017;57:125-154.
- Zhu YG, Feng XM, Abbott J, et al. Human mesenchymal stem cell microvesicles for treatment of Escherichia coli endotoxin-induced acute lung injury in mice. *Stem Cells*. 2014;32(1):116-125.

- 17. Monsel A, Zhu YG, Gennai S, et al. Therapeutic Effects of Human Mesenchymal Stem Cell-derived Microvesicles in Severe Pneumonia in Mice. *Am J Respir Crit Care Med*. 2015;192(3):324-336.
- 18. Willis GR, Fernandez-Gonzalez A, Reis M, et al. Mesenchymal stromal cell-derived small extracellular vesicles restore lung architecture and improve exercise capacity in a model of neonatal hyperoxia-induced lung injury. *J Extracell Vesicles*. 2020;9(1):1790874.
- 19. Yang S, Zhang K, Hou J, et al. Protective properties of extracellular vesicles in sepsis models: a systematic review and meta-analysis of preclinical studies. *J Transl Med*. 2023;21(1):262.
- 20. Zani-Ruttenstock E, Antounians L, Khalaj K, Figueira RL, Zani A. The Role of Exosomes in the Treatment, Prevention, Diagnosis, and Pathogenesis of COVID-19. *Eur J Pediatr Surg.* 2021;31(4):326-334.
- Pocsfalvi G, Mammadova R, Ramos Juarez AP, Bokka R, Trepiccione F, Capasso G.
 COVID-19 and Extracellular Vesicles: An Intriguing Interplay. *Kidney Blood Press Res.* 2020;45(5):661-670.
- 22. Can A, Celikkan FT, Cinar O. Umbilical cord mesenchymal stromal cell transplantations:

 A systemic analysis of clinical trials. *Cytotherapy*. 2017;19(12):1351-1382.
- 23. Barberi T, Willis LM, Socci ND, Studer L. Derivation of multipotent mesenchymal precursors from human embryonic stem cells. *PLoS Med.* 2005;2(6):e161.
- 24. Cesetti T, Fila T, Obernier K, et al. GABAA receptor signaling induces osmotic swelling and cell cycle activation of neonatal prominin+ precursors. *Stem Cells*. 2011;29(2):307-319.

- 25. Kang R, Zhou Y, Tan S, et al. Mesenchymal stem cells derived from human induced pluripotent stem cells retain adequate osteogenicity and chondrogenicity but less adipogenicity. *Stem Cell Res Ther*. 2015;6(1):144.
- 26. Ramos YFM, Tertel T, Shaw G, et al. Characterizing the secretome of licensed hiPSC-derived MSCs. *Stem Cell Res Ther.* 2022;13(1):434.
- 27. Bruschi M, Sahu N, Singla M, et al. A Quick and Efficient Method for the Generation of Immunomodulatory Mesenchymal Stromal Cell from Human Induced Pluripotent Stem Cell. *Tissue Eng Part A*. 2022;28(9-10):433-446.
- 28. Sabapathy V, Kumar S. hiPSC-derived iMSCs: NextGen MSCs as an advanced therapeutically active cell resource for regenerative medicine. *J Cell Mol Med*. 2016;20(8):1571-1588.
- 29. Xu M, Shaw G, Murphy M, Barry F. Induced Pluripotent Stem Cell-Derived Mesenchymal Stromal Cells Are Functionally and Genetically Different From Bone Marrow-Derived Mesenchymal Stromal Cells. Stem Cells. 2019;37(6):754-765.
- 30. Winston TS, Suddhapas K, Wang C, Ramos R, Soman P, Ma Z. Serum-Free Manufacturing of Mesenchymal Stem Cell Tissue Rings Using Human-Induced Pluripotent Stem Cells. *Stem Cells Int.* 2019;2019:5654324.
- 31. Winston TS, Chen C, Suddhapas K, et al. Controlling Mesenchyme Tissue Remodeling via Spatial Arrangement of Mechanical Constraints. *Front Bioeng Biotechnol*. 2022;10:833595.
- 32. Lewis AJ, Seymour CW, Rosengart MR. Current Murine Models of Sepsis. *Surg Infect* (*Larchmt*). 2016;17(4):385-393.

- 33. D'Alessio FR. Mouse Models of Acute Lung Injury and ARDS. *Methods Mol Biol.* 2018;1809:341-350.
- 34. Meng Q, Wang X, Guo D, et al. Nano-chemically Modified Tetracycline-3 (nCMT-3)

 Attenuates Acute Lung Injury via Blocking sTREM-1 Release and NLRP3

 Inflammasome Activation. *Shock.* 2022;57(5):749-758.
- 35. Hass R, Kasper C, Bohm S, Jacobs R. Different populations and sources of human mesenchymal stem cells (MSC): A comparison of adult and neonatal tissue-derived MSC. *Cell Commun Signal*. 2011;9:12.
- 36. Kim EY, Lee KB, Kim MK. The potential of mesenchymal stem cells derived from amniotic membrane and amniotic fluid for neuronal regenerative therapy. *BMB Rep.* 2014;47(3):135-140.
- 37. Cheng Y, Cao X, Qin L. Mesenchymal Stem Cell-Derived Extracellular Vesicles: A Novel Cell-Free Therapy for Sepsis. *Front Immunol.* 2020;11:647.
- 38. Spitzhorn LS, Megges M, Wruck W, et al. Human iPSC-derived MSCs (iMSCs) from aged individuals acquire a rejuvenation signature. *Stem Cell Res Ther.* 2019;10(1):100.
- 39. Ferreira JR, Teixeira GQ, Santos SG, Barbosa MA, Almeida-Porada G, Goncalves RM. Mesenchymal Stromal Cell Secretome: Influencing Therapeutic Potential by Cellular Pre-conditioning. *Front Immunol.* 2018;9:2837.
- 40. Ti D, Hao H, Tong C, et al. LPS-preconditioned mesenchymal stromal cells modify macrophage polarization for resolution of chronic inflammation via exosome-shuttled let-7b. *J Transl Med.* 2015;13:308.
- 41. Tolomeo AM, Zuccolotto G, Malvicini R, et al. Biodistribution of Intratracheal, Intranasal, and Intravenous Injections of Human Mesenchymal Stromal Cell-Derived

- Extracellular Vesicles in a Mouse Model for Drug Delivery Studies. *Pharmaceutics*. 2023;15(2).
- 42. Tieu A, Stewart DJ, Chwastek D, Lansdell C, Burger D, Lalu MM. Biodistribution of mesenchymal stromal cell-derived extracellular vesicles administered during acute lung injury. *Stem Cell Res Ther.* 2023;14(1):250.
- 43. Wiklander OP, Nordin JZ, O'Loughlin A, et al. Extracellular vesicle in vivo biodistribution is determined by cell source, route of administration and targeting. *J Extracell Vesicles*. 2015;4:26316.
- 44. Morrison TJ, Jackson MV, Cunningham EK, et al. Mesenchymal Stromal Cells Modulate Macrophages in Clinically Relevant Lung Injury Models by Extracellular Vesicle Mitochondrial Transfer. Am J Respir Crit Care Med. 2017;196(10):1275-1286.
- 45. Zhang D, Lee H, Wang X, Rai A, Groot M, Jin Y. Exosome-Mediated Small RNA Delivery: A Novel Therapeutic Approach for Inflammatory Lung Responses. *Mol Ther*. 2018;26(9):2119-2130.
- 46. Heo JS, Choi Y, Kim HO. Adipose-Derived Mesenchymal Stem Cells Promote M2 Macrophage Phenotype through Exosomes. *Stem Cells Int.* 2019;2019:7921760.
- 47. Xia L, Zhang C, Lv N, et al. AdMSC-derived exosomes alleviate acute lung injury via transferring mitochondrial component to improve homeostasis of alveolar macrophages. *Theranostics*. 2022;12(6):2928-2947.
- 48. Li L, Jin S, Zhang Y. Ischemic preconditioning potentiates the protective effect of mesenchymal stem cells on endotoxin-induced acute lung injury in mice through secretion of exosome. *Int J Clin Exp Med.* 2015;8(3):3825-3832.

- 49. Zhou Y, Li P, Goodwin AJ, et al. Exosomes from endothelial progenitor cells improve outcomes of the lipopolysaccharide-induced acute lung injury. *Crit Care*. 2019;23(1):44.
- 50. Wei X, Yi X, Lv H, et al. MicroRNA-377-3p released by mesenchymal stem cell exosomes ameliorates lipopolysaccharide-induced acute lung injury by targeting RPTOR to induce autophagy. *Cell Death Dis.* 2020;11(8):657.
- 51. Xu N, Shao Y, Ye K, et al. Mesenchymal stem cell-derived exosomes attenuate phosgene-induced acute lung injury in rats. *Inhal Toxicol*. 2019;31(2):52-60.
- 52. Wang X, Liu D, Zhang X, Yang L, Xia Z, Zhang Q. Exosomes from adipose-derived mesenchymal stem cells alleviate sepsis-induced lung injury in mice by inhibiting the secretion of IL-27 in macrophages. *Cell Death Discov.* 2022;8(1):18.
- 53. Chen W, Huang Y, Han J, et al. Immunomodulatory effects of mesenchymal stromal cells-derived exosome. *Immunol Res.* 2016;64(4):831-840.
- 54. Liu F, Peng W, Chen J, et al. Exosomes Derived From Alveolar Epithelial Cells Promote Alveolar Macrophage Activation Mediated by miR-92a-3p in Sepsis-Induced Acute Lung Injury. *Front Cell Infect Microbiol*. 2021;11:646546.
- 55. Liu JH, Li C, Cao L, Zhang CH, Zhang ZH. Exosomal miR-132-3p from mesenchymal stem cells alleviated LPS-induced acute lung injury by repressing TRAF6. *Autoimmunity*. 2021;54(8):493-503.
- 56. Liu X, Gao C, Wang Y, Niu L, Jiang S, Pan S. BMSC-Derived Exosomes Ameliorate LPS-Induced Acute Lung Injury by miR-384-5p-Controlled Alveolar Macrophage Autophagy. *Oxid Med Cell Longev.* 2021;2021:9973457.

- Wang X, Feng J, Dai H, et al. microRNA-130b-3p delivery by mesenchymal stem cellsderived exosomes confers protection on acute lung injury. *Autoimmunity*. 2022;55(8):597-607.
- 58. Zhang T, Lu L, Li M, et al. Exosome from BMMSC Attenuates Cardiopulmonary Bypass-Induced Acute Lung Injury Via YAP/beta-Catenin Pathway: Downregulation of Pyroptosis. *Stem Cells*. 2022;40(12):1122-1133.
- 59. Aguiar Koga BA, Fernandes LA, Fratini P, Sogayar MC, Carreira ACO. Role of MSC-derived small extracellular vesicles in tissue repair and regeneration. *Front Cell Dev Biol.* 2022;10:1047094.

Figure Legends

Fig.1. Accumulation of iMSC-EVs in organs after IT, IP and IV administration. *In vivo* Imaging System (IVIS 50) with the excitation/emission at 784/806 nm were used to longitudinally monitor iMSC-EVs trafficking in the organs including lung, heart, liver, kidney, spleen, stomach, and intestine.

Fig.2. Detection of uptake of iMSC-EVs in lung tissue and macrophages. The iMSC-EVs were labeled using ExoGlow-Vivo labeling kit from SBI. 50 μl of labeled iMSC-EVs was delivered into mice by IT. First, fresh lung tissue was collected and embedded and frozen in OCT after 24 h IT injection. Second, bronchoalveolar lavage fluid (BALF) was obtained from mouse lung and centrifuged. Lung tissue sections and slide with alveolar macrophages were visualized and shown in A and B. iMSC-EVs uptake in Raw264.7 macrophages was also detected by incubation of the cells and labeled iMSC-EVs for 4 h. Representative images are shown in C.

Fig. 3. Cytokine levels in plasma and bronchoalveolar lavage fluid (BALF). Mice were treated with iMSC-EVs (0.6 mg/kg) or vehicle 2 h before induction of endotoxemia by LPS (5 mg/kg, IP) and lung injury by LPS (2.5 mg/kg) using non-invasive tracheal installation by aerosolizer. Mice were sacrificed 24 h after LPS or saline, then BALF and plasma were collected for cytokines by ELISA. TNF-α and IL-6 from septic mice in plasma were shown in A and B. TNF-α (C & E) and IL-6 (D & F) in plasma and BALF were from the mice model of lung injury assayed. Scatter dot plot represents mean values and standard error of mean (SE) (n=4-6 / group).

Fig. 4. BALF cytology and total protein concentration. Mice were treated with iMSC-EVs (0.6 mg/kg) or vehicle 2 h before induction of lung injury by LPS (2.5 mg/kg) or sham lung injury (by saline) using non-invasive tracheal installation by aerosolizer. Mice were sacrificed 24 h after LPS or saline, then BALF was collected for examining neutrophils (black arrows) and macrophages (green arrows) by Hema 3 staining (A). Quantification of neutrophils (B) and macrophages (C) per slide were counted at ×400 magnification under light microscopy. Total protein concentration was assayed by BCA (D). Scatter dot plot represents mean values and standard error of mean (SE) (n=4-6 / group).

Fig. 5. Histological assessment of lung injury. Mice were treated with iMSC-EVs (0.6 mg/kg) or vehicle 2 h before induction of lung injury by LPS (2.5 mg/kg) or sham lung injury (by saline) using non-invasive tracheal installation by aerosolizer. Mice were sacrificed 24 h after LPS or saline, then lung tissue was collected for H&E staining to evaluate lung injury from each group (A). Lung injury was characterized by neutrophil infiltration (red arrows), hyaline membranes, proteinaceous debris filling the airspaces and alveolar septal thickening (black arrows). Semi-quantitative histological lung injury score was assessed (B). Scatter dot plot represents mean values and standard error of mean (SE) (n=4-6 / group).

Fig. 6. Kaplan-Meier survival analysis of septic mice treated with iMSC-EVs. Mice were treated with iMSC-EVs (0.6 mg/kg) or vehicle 2 h before induction of endotoxemia by LPS (5 mg/kg, IP). Then, the mice were observed for 3 days, and the survival and dead mice were counted. Black, blue and red curves represent survival probability in control (N=8), LPS

(N=15) and LPS plus iMSC-EVs (N=15) groups. Log-Rank Test were used to compare the difference in survival probability during 3-day observation period.

Fig. 7. Cytokine levels in plasma and BALF, and histological assessment of lung injury in a murine model with therapeutic administration of iMSC-EVs. Mice were treated with iMSC-EVs (0.6 mg/kg) or vehicle 2 h after induction of lung injury by LPS (2.5 mg/kg) or sham lung injury (by saline) using non-invasive tracheal installation by aerosolizer. Mice were sacrificed 24 h after LPS or saline, then plasma, BALF and lung tissue were collected for cytokine analysis and H&E staining to evaluate inflammation (A) and lung injury (B) from each group. Lung injury was characterized by neutrophil infiltration (red arrows), hyaline membranes, proteinaceous debris filling the airspaces and alveolar septal thickening (black arrows). Semi-quantitative histological lung injury score was assessed. Scatter dot plot represents mean values and standard error of mean (SE) (n=3-4 / group).

Figure 1

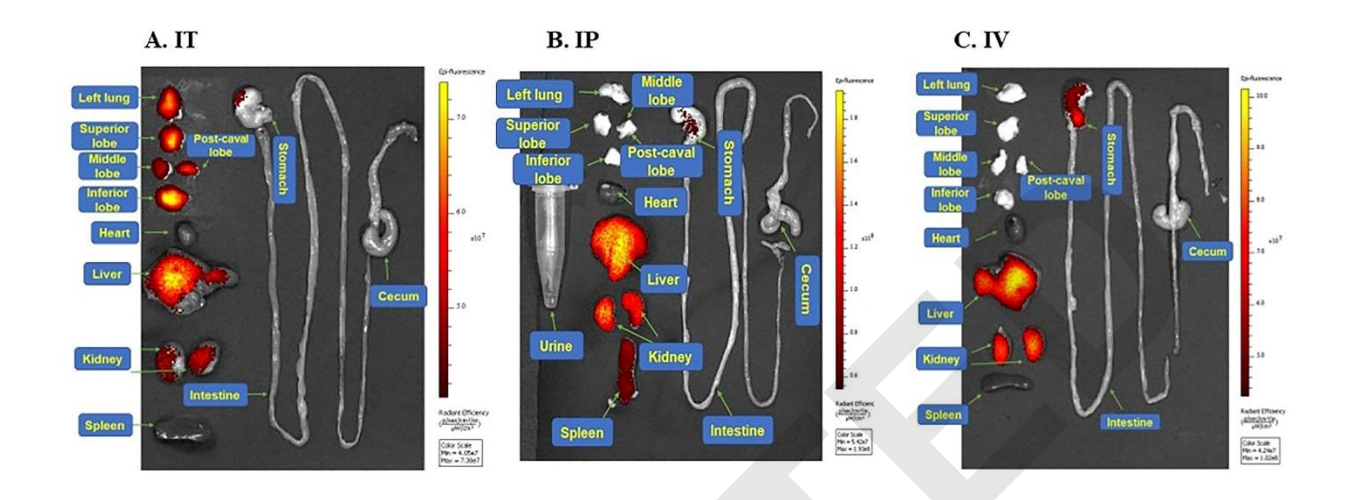


Figure 2

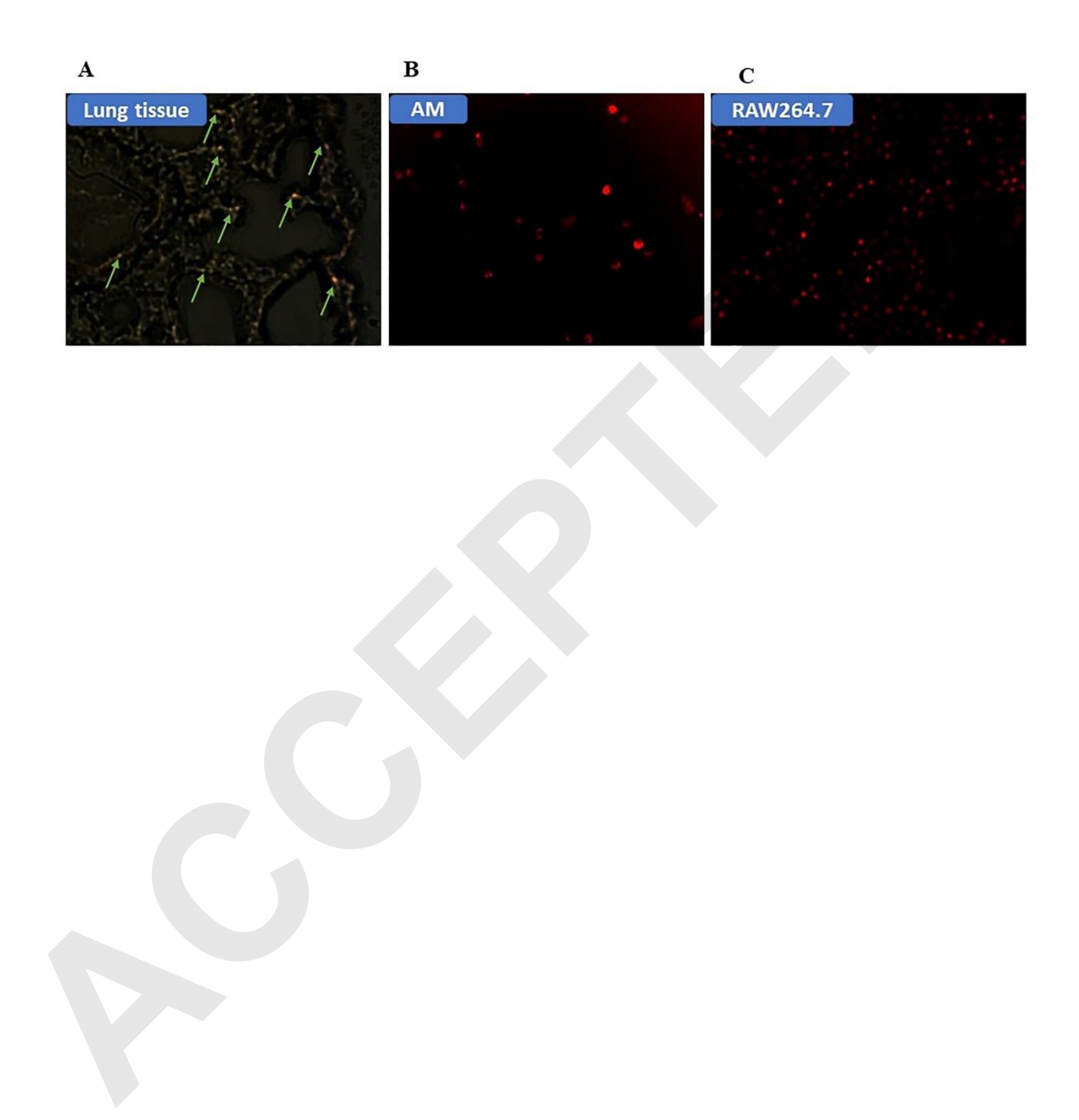


Figure 3

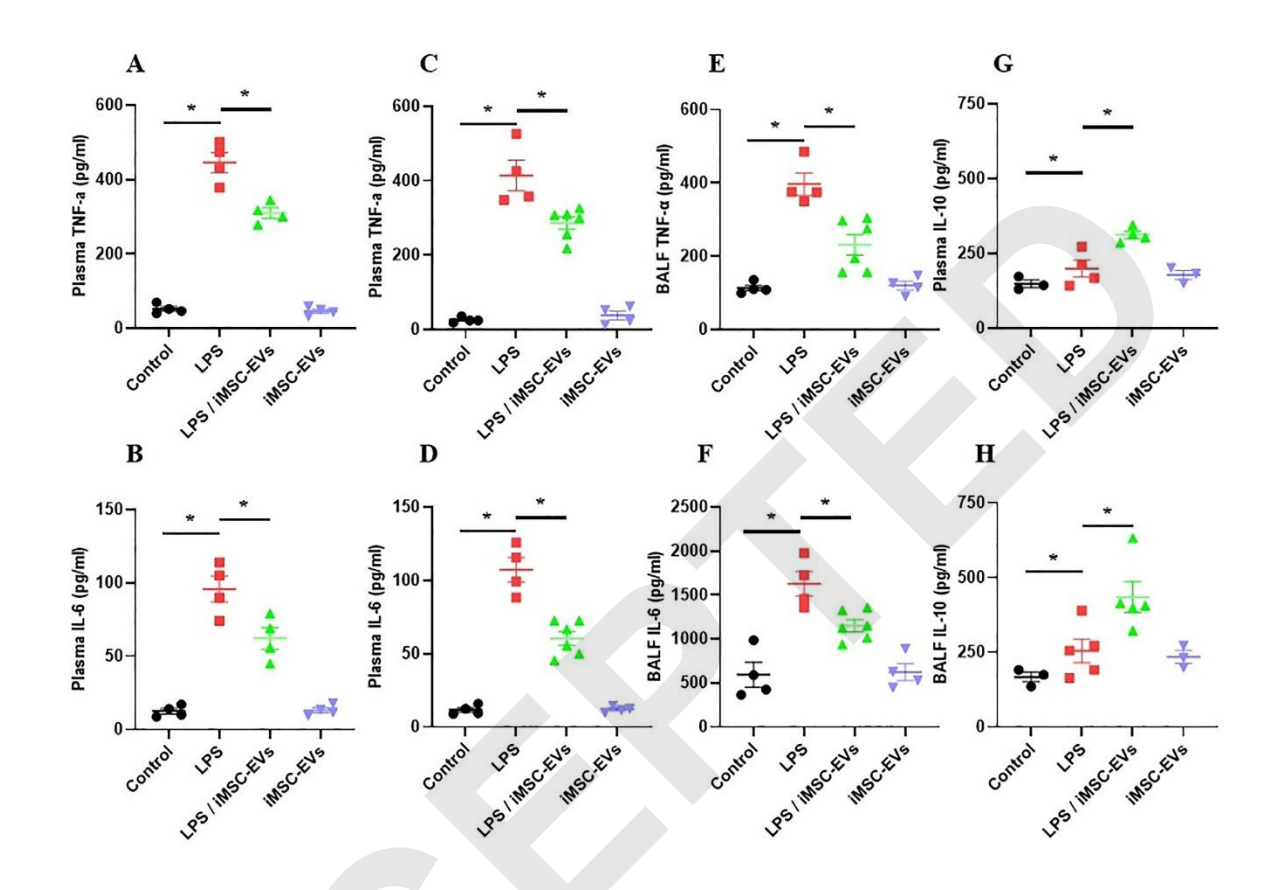


Figure 4

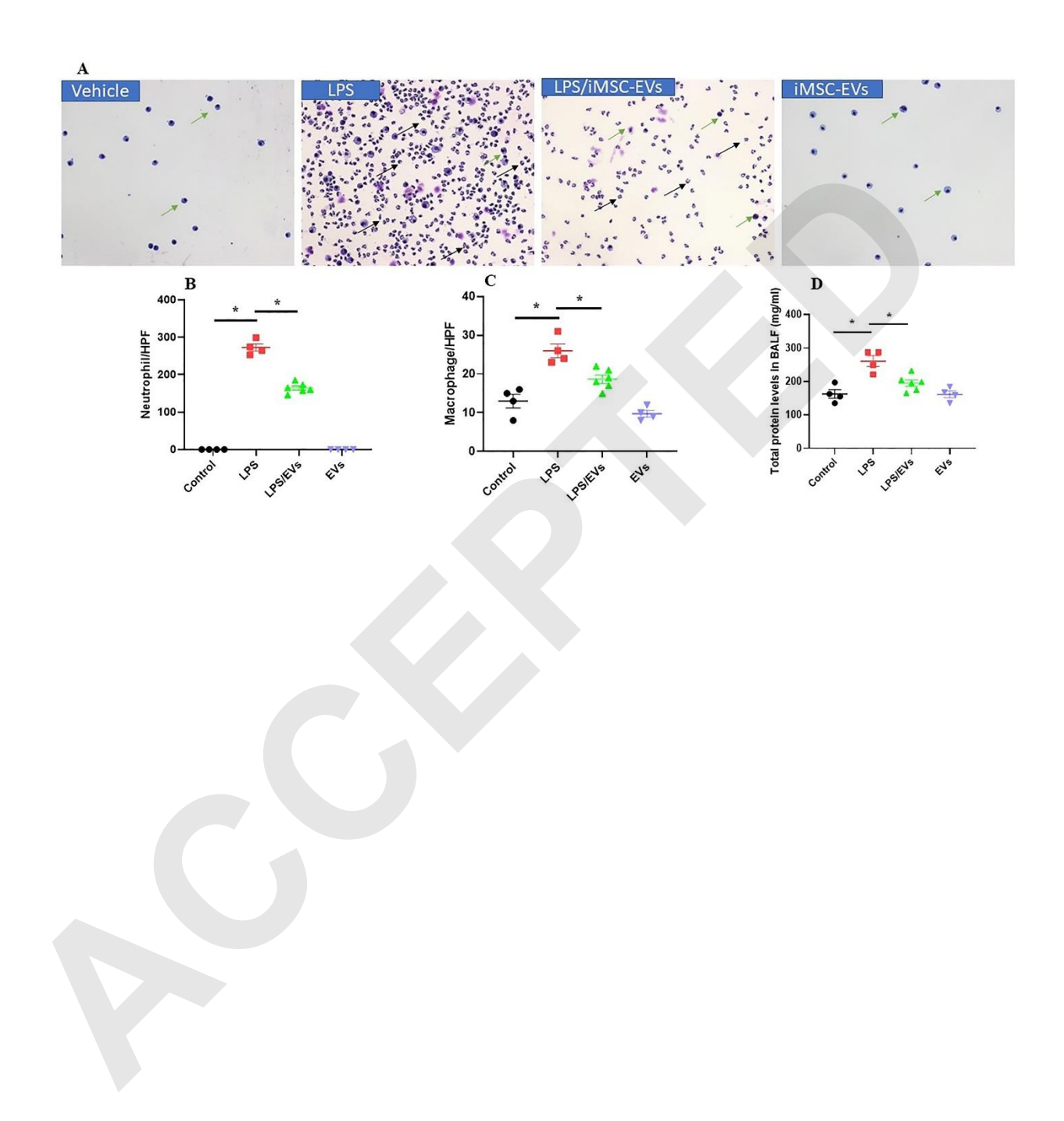


Figure 5

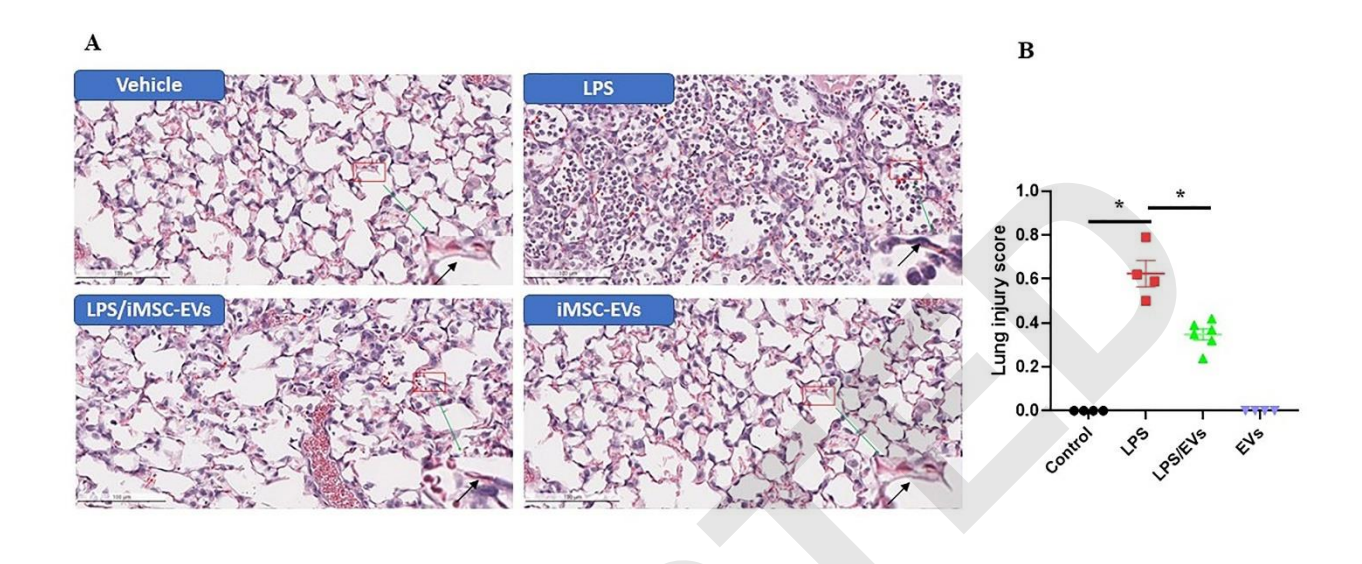
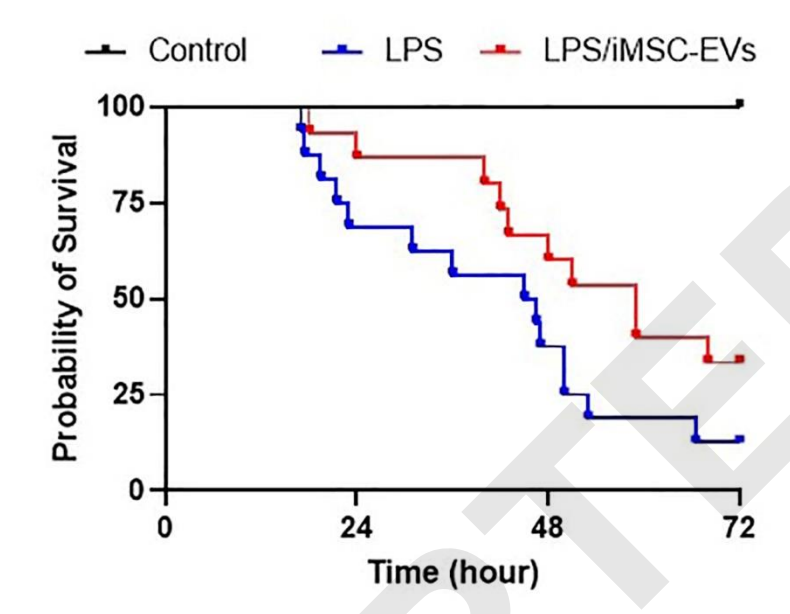
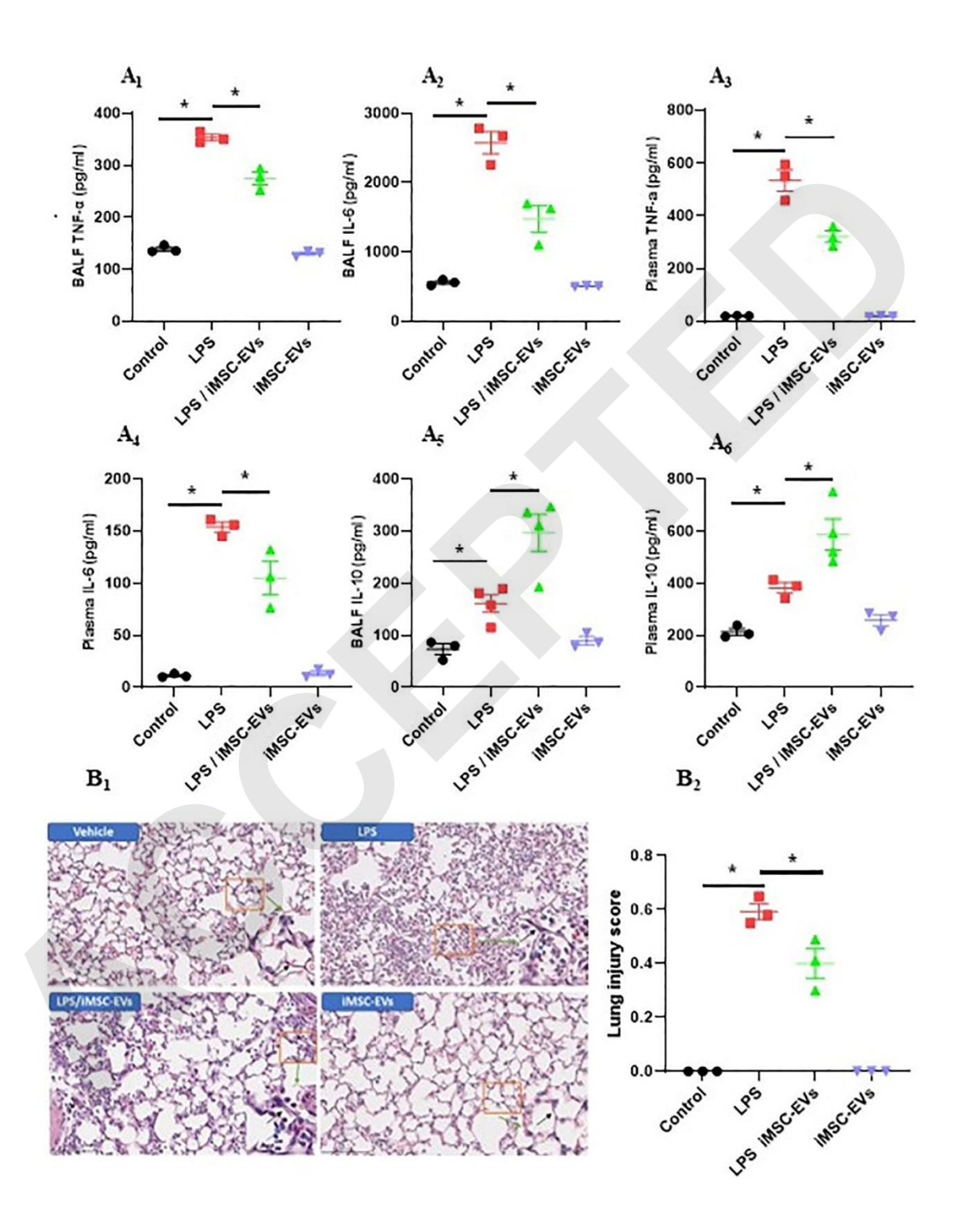


Figure 6

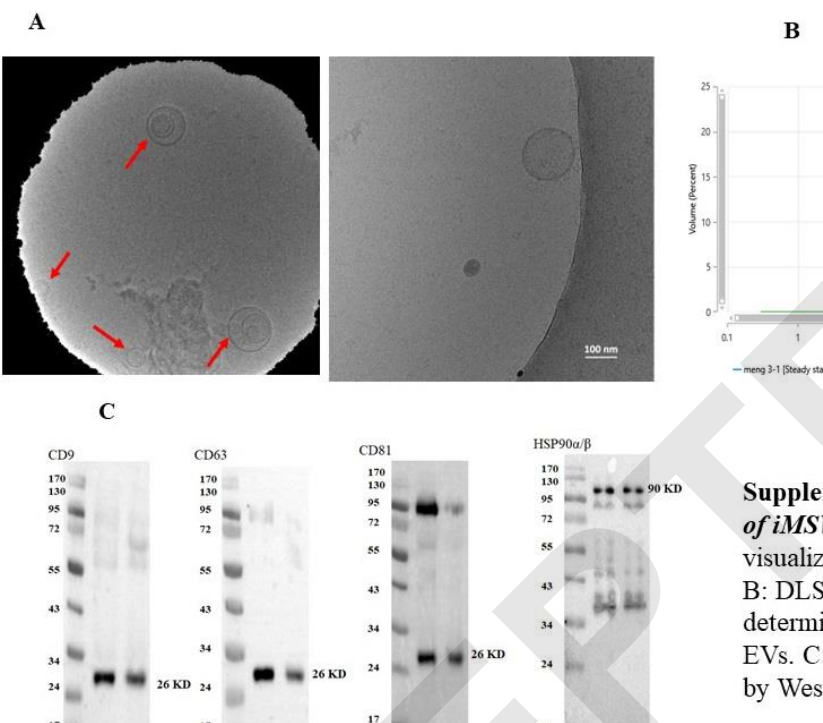


Log-rank (mantel-Cox) Test, P=0.0004

Figure 7



Supplemental Figure 1



Supplemental Figure-1. Identification of iMSV-EVs: TEM was employed to visualize the morphology of iMSC-EVs. B: DLS analysis was performed to determine the size distribution of iMSC-EVs. C: EV marker expression detected by Western Blot.

Supplemental Figure 2

